

Evanescent Wave Cavity Ring-Down  
Spectroscopy as a probe of Interfacial  
Adsorption: Interaction of tris(2,2'-  
bipyridine)ruthenium(II) with silica surfaces and  
polyelectrolyte films

*Hayley V. Powell<sup>1</sup>, Mathias Schnippering<sup>1</sup>, Mikhail Mazurenka<sup>2</sup>, Julie V. Macpherson<sup>1</sup>,  
Stuart R. Mackenzie<sup>2\*</sup> and Patrick R. Unwin<sup>1\*</sup>*

<sup>1</sup>Department of Chemistry, University of Warwick, Gibbet Hill Road, Coventry, CV4 7AL

<sup>2</sup>Department of Chemistry, University of Cambridge, Lensfield Road, Cambridge, CB2

1EW

Email: srm49@cam.ac.uk, p.r.unwin@warwick.ac.uk.

ABSTRACT Evanescent wave cavity ring-down spectroscopy (EW-CRDS) has been used to study the interaction of the tris(2,2'-bipyridine)ruthenium(II) complex,  $[\text{Ru}(\text{bpy})_3]^{2+}$ , at both native silica surfaces and surfaces modified with polyelectrolyte films. Both poly-L-lysine (PLL) and a PLL/poly-L-glutamic acid (PGA) bilayer functionalized interfaces have been studied. Concentration isotherms exhibit Langmuir type adsorption behavior on both silica and PGA-terminated surfaces from which equilibrium constants have been derived. The pH-dependence of the  $[\text{Ru}(\text{bpy})_3]^{2+}$  adsorption to silica and the PLL/PGA film has also been investigated. For the latter substrate, the effective surface  $pK_a$  of the acid groups was found to be 5.5. The effect of supporting electrolyte was also investigated and shown to have a significant effect on the extent of  $[\text{Ru}(\text{bpy})_3]^{2+}$  adsorption. A thin layer electrochemical cell arrangement, in which a working electrode was positioned just above the substrate, was used to change the solution pH in a controlled way via the potential-pulsed chronoamperometric oxidation of water. By measuring the optical absorption using EW-CRDS during such experiments, the desorption of  $[\text{Ru}(\text{bpy})_3]^{2+}$  from the surface has been monitored in real time. Experiments were carried out at different cell thicknesses and at various pulse durations. By combining data from the EW-CRDS experiments with fluorescence confocal laser scanning microscopy (CLSM) to determine the pH at the substrate surface, the  $pK_a$  of the PLL/PGA film could be ascertained and was found to agree with the static pH isotherm measurements. These studies provide a platform for the further use of electrochemistry combined with EW-CRDS to investigate dynamic processes at interfaces.

KEYWORDS interfacial spectroscopy, cavity ring-down, evanescent wave, adsorption, desorption, spectroelectrochemistry,  $[\text{Ru}(\text{bpy})_3]^{2+}$

## Introduction

Adsorption/desorption processes are fundamental to a wide range of phenomena across the physical sciences, the life sciences and in environmental science.<sup>1-8</sup> Furthermore, adsorption at solid/liquid interfaces is an essential feature of many industrial processes such as heterogeneous catalysis, purification and chemical separation.<sup>9</sup> Sensitive techniques which can probe adsorption at interfaces, particularly *in-situ* methods with high temporal, spatial and spectral resolution, are valued highly as providing a route to a better understanding of these important processes.

The kinetics of potential-dependent adsorption/desorption at electrified interfaces are usually readily measured, because one can exercise control of the interfacial process via the applied potential and follow the adsorption process via the current response and/or the response from other traditional surface science techniques.<sup>10-17</sup> For electrically insulating interfaces, the study of adsorption/desorption processes, especially under dynamic control, is more challenging due to the need to introduce/remove the adsorbate into a solution on a rapid timescale and follow the subsequent interfacial process. Temperature jump,<sup>18</sup> stopped flow<sup>19-22</sup> and pressure jump methods<sup>23-25</sup> have been applied successfully to suspensions of solid materials in solution, but studies of macroscopic interfaces have been rather limited. Progress in this area has been made through the use of electrochemical techniques coupled to insulating surfaces, such as channel flow electrode methods<sup>26</sup> and scanning electrochemical microscopy (SECM)<sup>27-30</sup> and related methods<sup>30</sup>, which have been used to determine rate constants and equilibrium constants of several adsorption/desorption processes. These methods tend to utilize a strategically placed electrode, located in a solution phase close to the interface of interest to introduce/remove an adsorbate and to follow the adsorption/desorption process. The development of this

approach by the incorporation of complementary surface-sensitive spectroscopic techniques would be expected to provide enhanced information on such processes.

Cavity ring-down spectroscopy (CRDS) has developed as an ultra-sensitive gas-phase absorption technique.<sup>31-34</sup> Recently, CRDS has been successfully transferred into the condensed phase, either by placing the solution inside the cavity, involving direct contact of the solution with the mirrors,<sup>35, 36</sup> coating the mirrors with the species of interest<sup>37</sup> or by inserting a cell at the Brewster angle.<sup>38-40</sup> Pipino *et al.* were the first to probe surface specific processes using evanescent wave cavity ring-down spectroscopy (EW-CRDS).<sup>41</sup> In its simplest form this technique involves coupling a pulsed laser beam into an optical cavity, consisting of two high reflectivity mirrors and a fused silica prism and detecting the decay in the light level within the cavity once the laser is switched off. An evanescent field is created when the laser beam undergoes total internal reflection in the prism, whose amplitude decays exponentially with distance from the boundary. Since this evanescent field extends only  $\sim \lambda/2$  beyond the interface, it can be used to investigate the absorbance properties of the liquid phase in the first few hundred nanometers of solution above the silica prism surface, rendering it ideal for studying interfacial phenomena.

Besides those described, a wide range of different cavity geometries have been developed<sup>41-57</sup> which have been applied to fields as diverse as sub-monolayer detection,<sup>53</sup> investigations of the orientation of adsorbates at the gas/solid interface,<sup>42, 43</sup> and vibrational overtone spectroscopy.<sup>42</sup> Among applications at the solid/solution boundary, early studies have focused on adsorption processes at the silica/liquid interface. For example, the interaction of different dye molecules with the silica surface,<sup>44-46</sup> and the adsorption of other organic molecules have been studied.<sup>47,48</sup> In these cases, submonolayer detection of adsorbates has been achieved.

While the majority of previous studies of adsorption have focused on the silica prism inherent in EW-CRDS, this can be modified in various ways, thereby expanding the range of surfaces that can be investigated. As exemplified herein, multilayer assemblies of polyelectrolytes such as poly-L-lysine (PLL) and poly-L-glutamic acid (PGA) can be deposited, thereby changing the properties of the surface and facilitating the study of different electrostatic interactions. Some initial studies using this type of surface modification to study nanoparticle adsorption and dissolution by EW-CRDS have recently been reported by us.<sup>58, 59</sup>

Tris(bipyridine)ruthenium(II) ( $[\text{Ru}(\text{bpy})_3]^{2+}$ ) is a widely used reagent in electrochemiluminescence (ECL) analysis.<sup>60, 61</sup> Many efforts have been made to transfer  $[\text{Ru}(\text{bpy})_3]^{2+}$  directly to sensing electrodes in order to obtain reusable and simple detection devices. For example,  $[\text{Ru}(\text{bpy})_3]^{2+}$  has been immobilized into sol-gel systems such as titania,<sup>62</sup> ultrathin polymer films such as Nafion<sup>63, 64</sup> or on metal nanoparticles,<sup>65, 66</sup> carbon nanotubes composites<sup>67-69</sup> and nanotube electrodes.<sup>69</sup> Immobilized ruthenium complexes are also used extensively in dye sensitized solar cells<sup>70</sup>. Clearly, knowledge of the adsorption properties of  $[\text{Ru}(\text{bpy})_3]^{2+}$  is important for optimizing these many and varied applications.

We have previously demonstrated the application of EW-CRDS to monitor electrogenerated species within an electrochemical cell during cyclic voltammetry and chronoamperometry.<sup>49</sup> These studies highlighted the capability of EW-CRDS to follow dynamic processes in real time. In this article we present a study of the surface adsorption of  $[\text{Ru}(\text{bpy})_3]^{2+}$  onto both bare silica and silica functionalized with polyelectrolyte films. The effect of solution pH on adsorption was investigated both by changing the bulk solution and, more locally, by electrochemically-induced pH jumps (via water oxidation), employing a macroelectrode close to the prism surface in a thin layer electrochemical cell

arrangement. This latter procedure allowed the desorption process to be followed quantitatively in real time and, combined with pH-determination via fluorescence confocal laser scanning microscopy,<sup>71</sup> provided a rapid method for monitoring the surface coverage of  $[\text{Ru}(\text{bpy})_3]^{2+}$  as a function of pH. These studies provide a platform for future studies of surface dynamics using EW-CRDS.

## Experimental

**Apparatus for EW-CRDS.** The cavity ring-down spectrometer used has been described elsewhere<sup>58, 59</sup> and is shown in Figure 1. The cavity consisted of two high-reflectance concave mirrors ( $R = 99.997\%$  at 405 nm, Los Gatos Research). The mirrors, with radii of curvature of 1 m, were mounted in adjustable gimbal mounts separated by 28 cm and 36 cm for experiments on polymer-modified prisms and silica, respectively. The third element of the cavity was a standard commercial right-angle fused-silica prism (CVI and Laser Components) antireflection coated (AR,  $R < 0.5\%$ ) on the non-hypotenuse surfaces. The prism and the mirrors were mounted on a commercially available breadboard (Thorlabs). A pulsed laser (Power Technology Inc., 405 nm, 50 mW maximum output, linewidth *ca.* 1 nm) was employed. The laser was pulsed at a frequency of 2.4 kHz with an external pulse generator (TTi, TGP110). The use of the “broadband”, rapid-pulsed diode laser negates the need for the acousto-optic modulator used to chop the narrow linewidth laser used in our earlier paper<sup>49</sup> and permitted the much faster repetition rates used here. The cavity was aligned following the procedure described previously.<sup>49</sup> A photomultiplier tube (Electron Tubes, 9781B) was used to measure the light intensity reflected from the incident prism surface, rather than the light transmitted through the mirrors due to a higher percentage of intracavity intensity at this location.

The equilibrium adsorption experiments were carried out using a cuboid cell fitted with inlets at both ends to permit flushing between each experiment. The cell used for the combined electrochemical and spectroscopic measurements was described previously.<sup>49</sup> The working electrode (2.0-mm-diameter circular platinum electrode with an overall diameter, including insulation, of 6.35 mm) was placed over the region of the prism probed by the evanescent field, using a 3-axis micropositioner. The distance between the working electrode and the prism surface was chosen to be between 200 to 500  $\mu\text{m}$  so that the electrode did not penetrate the evanescent field and thus did not affect the EW-CRDS signal. The evanescent field penetration depth was calculated to be 242 nm for experiments on silica.

**Data analysis.** The cavity ring-down signal was recorded on a 12-bit 400 MS/s oscilloscope card (Gage CS12400) and the cavity ring-down time from each transient was calculated with the fast Fourier transform method<sup>72</sup> using custom-written LabVIEW software. Ring-down times were typically smoothed using 100 point adjacent averaging. The electrochemical data were recorded onto a National Instruments PCI-6221 card simultaneously using the same LabVIEW program to ensure data synchronization.

**Adsorption experiments.** Tris(2,2'-bipyridine) dichlororuthenium(II) was purchased from Sigma-Aldrich and stored in the dark. Solutions of different concentrations and pH values were freshly prepared prior to experiments. The pH was adjusted using HCl (Fisher Scientific) or HClO<sub>4</sub> (Acros) and NaOH (Fisher Scientific).

The surfaces investigated were either bare fused silica or polymer-modified fused silica. For experiments on fused silica, adsorption isotherms at two different pH values (2.7 and 6.7) were recorded over a wide range of concentrations and were recorded in random order. Additionally, the pH-dependence of the adsorption was investigated at a fixed concentration of 1 mM [Ru(bpy)<sub>3</sub>]<sup>2+</sup>, with and without supporting electrolyte (0.1 M NaCl,



Aldrich). Between each measurement the cell was rinsed with ultra pure Milli-Q water until the background ring-down signal was recovered, indicating that the prism surface was clean. UV-visible absorption spectra recorded at different pH values confirmed no pH dependence of the optical absorbance of  $[\text{Ru}(\text{bpy})_3]^{2+}$  with the molar extinction coefficient changing by less than 1% in the range pH 2-11.

For studies of modified surfaces, the basal surface of the prism was coated with PLL (Sigma-Aldrich) using the drop coating method. The film was deposited from  $1 \text{ mg mL}^{-1}$  solutions for adsorption times of 20 min. After adsorption of the polymer, the prisms were rinsed with ultra pure Milli-Q water and dried in an air flow. This yielded an intrinsically positively charged surface. The same procedure was used to deposit a PGA film (Sigma-Aldrich) onto a previously deposited PLL film in order to achieve a negatively charged surface onto which  $[\text{Ru}(\text{bpy})_3]^{2+}$  would be strongly adsorbed (along with the supporting electrolyte cation). Isotherms and pH-dependence experiments for the adsorption of  $[\text{Ru}(\text{bpy})_3]^{2+}$  onto these functionalized surfaces were performed with and without supporting electrolyte (50 mM tetrabutylammonium chloride, TBACl, Sigma-Aldrich). This supporting electrolyte was selected as the tetrabutylammonium cation ( $\text{TBA}^+$ ) is likely to bind less competitively than a cation of higher charge density, such as the sodium ion.<sup>73</sup> After every experiment, the prisms were cleaned in oxygen plasma for 20 min at 100 W (Emitech, K1050X) with the anti-reflection coatings covered and wiped with methanol (Aldrich, spectroscopy grade).

**Electrochemically-induced desorption.** Chronoamperometric experiments were performed using a homebuilt potentiostat with a Pt working electrode ( $\varnothing = 2 \text{ mm}$ ), a Pt wire counter electrode and a Ag wire coated in AgCl which acted as a Ag/AgCl (saturated AgCl) reference electrode.<sup>74</sup> The potential of the working electrode was stepped from 0.2 V, where no processes occurred, to 1.2 V for a defined period in order to generate protons

via water oxidation, thereby decreasing the pH within the thin layer cell from a bulk value,  $7 < \text{pH} < 8$ , in a well-defined manner. At the end of the step the potential was stepped back to 0.2 V. The effects of the duration of the potential step and the prism/electrode separation were examined.

**Fluorescence confocal laser scanning microscopy (CLSM).** CLSM measurements of the pH in the thin layer cell were carried out in an arrangement which mimicked the EW-CRDS measurements, using a cuboidic cell in which a glass substrate was positioned opposite the Pt working electrode described in the previous section. The cell was positioned on the stage of a Zeiss LSM 510, Axioplan 2, confocal microscope. An Argon laser ( $\lambda = 488 \text{ nm}$ ) was used for the excitation of  $10 \text{ }\mu\text{M}$  fluorescein (Sigma-Aldrich) whose fluorescence was measured in conjunction with a long pass filter ( $\lambda = 505 \text{ nm}$ ). Line scans between the electrode and substrate along the central axis of symmetry of the electrode were obtained every 5 ms, while the potential was stepped in the same manner as for the electrochemically-induced desorption experiments. The supporting electrolyte was 50 mM TBACl and the initial pH of the fluorescein solution was adjusted to 8 using NaOH and  $\text{HClO}_4$ . This ensured that the CLSM measurements matched the EW-CRDS measurements and also allowed the pH to be determined with optimal precision.<sup>71</sup> The same electrode-substrate separations and potential step times as for the electrochemical-induced desorption experiments were investigated. By measuring the spatially-resolved fluorescence profiles as a function of time it was possible to obtain detailed information on the evolution of  $\text{pH}^{71, 75, 76}$  in the thin layer cell.

## Results and Discussion

**Bulk Absorbance.** The bulk optical absorbance was obtained for  $[\text{Ru}(\text{bpy})_3]^{2+}$  in solution with a PLL-modified prism surface, on which there was no detectable  $[\text{Ru}(\text{bpy})_3]^{2+}$  adsorption, so that the optical absorbance,  $A$ , with concentration followed the Beer-Lambert law (Figure 2). The experimental data were fitted to a straight line which intercepted the origin, with a slope  $B$  corresponding to  $\varepsilon d_{\text{eff}}$  where  $\varepsilon$  is the molar absorption coefficient at the wavelength of 405 nm and  $d_{\text{eff}}$  the effective path length.

$$A = B c_{\text{Ru}} = \varepsilon d_{\text{eff}} c_{\text{Ru}} \quad (1)$$

The gradient of the line was  $(0.677 \pm 0.012) \text{ M}^{-1}$  for  $[\text{Ru}(\text{bpy})_3]^{2+}$  in pure water and  $(0.727 \pm 0.009) \text{ M}^{-1}$  for  $[\text{Ru}(\text{bpy})_3]^{2+}$  in 50 mM TBACl. The difference in the two gradients can be attributed to the slight variation in extinction coefficients at 405 nm for  $[\text{Ru}(\text{bpy})_3]^{2+}$  in pure water ( $\varepsilon_{405} = 6270 \text{ dm}^3 \text{ mol}^{-1} \text{ cm}^{-1}$ ) and for  $[\text{Ru}(\text{bpy})_3]^{2+}$  in 50 mM TBACl ( $\varepsilon_{405} = 6630 \text{ dm}^3 \text{ mol}^{-1} \text{ cm}^{-1}$ ). From the slope of the fitting function displayed in Figure 2, it was possible to derive an effective optical path length of  $1.08 \mu\text{m}$  which is in fairly good agreement with the effective path length calculated from theory using a low absorption approximation<sup>77</sup>. There was apparently no strong dependence of the effective path length on the electrolyte concentration. The values reported for the slopes were used to correct for the bulk absorbance in the other experiments (*vide infra*).

**Equilibrium Adsorption on Silica.** The adsorption of  $[\text{Ru}(\text{bpy})_3]^{2+}$  on negatively charged surfaces could be promoted on electrostatic grounds, although to the best of our knowledge there have been no previous reports of the adsorption of  $[\text{Ru}(\text{bpy})_3]^{2+}$  on glass or silica surfaces. The equilibrium adsorption was measured as a function of the bulk concentration of  $[\text{Ru}(\text{bpy})_3]^{2+}$ . Figure 3A shows the optical absorbance with time in the evanescent field after the injection (at  $t = 0$ ) of  $[\text{Ru}(\text{bpy})_3]^{2+}$  solutions at pH 2.7 (0.5 mM and 1 mM) and 6.7 (1 mM) into the sample cell with an unmodified silica prism. In each

case, there is a rapid rise in absorbance due to  $[\text{Ru}(\text{bpy})_3]^{2+}$  in solution and, in principle, adsorbed on the silica surface. The long time absorbance values for various  $[\text{Ru}(\text{bpy})_3]^{2+}$  concentrations and solution pH were obtained by averaging the steady-state values from the long-time plateaus of data such as that in Figure 3A. By comparing the data in Figure 3A for 1 mM at pH 2.7 and 6.7 it is evident that higher pH (more negatively charged silica surface) leads to higher optical absorbance, which can be attributed to the more significant adsorption of  $[\text{Ru}(\text{bpy})_3]^{2+}$  on the more highly charged surface. The concentration dependence of the optical absorption is also evident from the data for 0.5 mM and 1.0 mM  $[\text{Ru}(\text{bpy})_3]^{2+}$  at pH 2.7.

Figure 3B shows the concentration dependence of the optical absorbance of  $[\text{Ru}(\text{bpy})_3]^{2+}$  at pH 2.7 and pH 6.7 for concentrations up to 3 mM. For both pH values, the absorbance increases with concentration, as would be expected, due to bulk absorbance; but the morphology of the absorbance-concentration curves are clearly strongly pH-dependent. Given the independence of the  $[\text{Ru}(\text{bpy})_3]^{2+}$  absorbance on pH, the higher interfacial absorbance values at pH 6.7 suggest the enhanced accumulation of  $[\text{Ru}(\text{bpy})_3]^{2+}$  on the surface at this pH. It is possible to fit the pH 2.7 data to a linear function, because the degree of dissociation of silanol groups is very small at this pH and practically all the optical absorbance originates from  $[\text{Ru}(\text{bpy})_3]^{2+}$  in bulk solution. The slope of the fitted linear function is  $(0.670 \pm 0.096) \text{ M}^{-1}$ , which agrees very well with the previously obtained values for the bulk absorbance of  $[\text{Ru}(\text{bpy})_3]^{2+}$  measured with a PLL-modified silica surface. For negatively charged surfaces (at higher pH), the absorbance measured by EW-CRDS has two components: i) interfacial, due to surface-adsorbed  $[\text{Ru}(\text{bpy})_3]^{2+}$  and ii) bulk due to the penetration of the evanescent field into solution as discussed above.

In the discussion of the above results one must take account of the surface  $pK_a$  of silica functional groups, which are broadly of two types:<sup>44, 50</sup> 19% with a  $pK_a$  value of ca. 8.5

and 81% with a  $pK_a$  value of ca. 4.5. At pH 6.7,  $[\text{Ru}(\text{bpy})_3]^{2+}$  will adsorb overwhelmingly on those silanol groups with  $pK_a$  4.5, with negligible adsorption on the sites characterized by the higher  $pK_a$ . The experimental pH 6.7 data were therefore fitted to a single Langmuir function, using  $A_{\text{max}}$  (the maximum optical absorbance at pH 6.7 arising from adsorbed  $[\text{Ru}(\text{bpy})_3]^{2+}$  when all the adsorption sites are occupied) and the equilibrium constant,  $K$ , as fitting parameters. The function naturally included the bulk absorbance, using the gradient,  $B$ , obtained from measurements on PLL (or silica at pH 2.7):

$$A = \frac{A_{\text{max}} K C_{\text{Ru}}}{1 + K C_{\text{Ru}}} + B C_{\text{Ru}} \quad (2)$$

From the fit, the absorbance due to adsorbed  $[\text{Ru}(\text{bpy})_3]^{2+}$  on silica at pH 6.7 was found to be  $A_{\text{max}} = (9.50 \pm 0.06) \times 10^{-4}$  and the equilibrium constant  $K = (1.72 \pm 0.30) \times 10^3 \text{ M}^{-1}$ . For the range of bulk  $[\text{Ru}(\text{bpy})_3]^{2+}$  concentrations investigated, the surface coverage varied from  $7.94 \times 10^{-13} \text{ mol cm}^{-2}$  to  $1.20 \times 10^{-10} \text{ mol cm}^{-2}$ . These submonolayer coverages highlight the extreme surface sensitivity of the EW-CRDS method, especially given that the wavelength of the laser used (405 nm) is some way removed from  $\lambda_{\text{max}}$  of  $[\text{Ru}(\text{bpy})_3]^{2+}$  (453 nm).

With the assumptions outlined, the total density of silanol groups,  $\Gamma$ , on the prism surface can be obtained from<sup>44</sup>

$$A_{\text{max}} = \Gamma \varepsilon r \alpha, \quad (3)$$

where  $r$  is the fraction of sites that have  $pK_a$  4.5 and  $\alpha$  is the degree of dissociation of these sites at pH 6.7 (99 %). According to Fisk et al.<sup>44</sup> the fraction of these sites is 0.272 which gives  $\Gamma = 5.53 \times 10^{-10} \text{ mol cm}^{-2}$  or 3.3 groups  $\text{nm}^{-2}$ , which is in good agreement with previous results.<sup>44, 78, 79</sup>

In order to investigate the pH-dependence of  $[\text{Ru}(\text{bpy})_3]^{2+}$  adsorption on bare fused silica more fully, the surface concentration of  $[\text{Ru}(\text{bpy})_3]^{2+}$  was measured as a function of pH from a solution containing 1 mM  $[\text{Ru}(\text{bpy})_3]^{2+}$  in both pure water and with 0.1 M NaCl. The results in Figure 4, which show only adsorbed  $[\text{Ru}(\text{bpy})_3]^{2+}$  (after subtraction of optical absorption due to solution), show that in the pH 1-7 range, the surface concentration of  $[\text{Ru}(\text{bpy})_3]^{2+}$  increases with increasing pH due to the increasing deprotonation of silanol groups and the consequent increase in the number of possible adsorption sites. At higher pH, the surface concentration actually falls again (at around pH 11 for  $[\text{Ru}(\text{bpy})_3]^{2+}$  in water and pH 8 for the high ionic strength solution) which can be attributed to an increase in the ionic strength due to the addition of NaOH used to increase the pH.  $\text{Na}^+$  ions appear to compete effectively with the  $[\text{Ru}(\text{bpy})_3]^{2+}$  to bind to available silanol groups and thus at higher pH (higher  $[\text{Na}^+]$ ) fewer  $\text{SiO}^-$  sites are free to bind  $[\text{Ru}(\text{bpy})_3]^{2+}$ . The same effect is seen for  $[\text{Ru}(\text{bpy})_3]^{2+}$  in 0.1 M NaCl; the drop in  $[\text{Ru}(\text{bpy})_3]^{2+}$  surface concentration occurs at around pH 8 due to the fact that NaCl is already present as a supporting electrolyte.

**Adsorption on PLL/PGA bilayers.** Isotherms for  $[\text{Ru}(\text{bpy})_3]^{2+}$  adsorption on a PLL/PGA bilayer, with and without supporting electrolyte (50 mM TBACl) at pH 8, are shown in Figure 5. Both isotherms were obtained from optical absorbance measurements of the type already described, which were corrected for the bulk absorbance and then divided by  $\epsilon$  to reveal the amount of  $[\text{Ru}(\text{bpy})_3]^{2+}$  on the surface. Compared to the isotherms for silica at pH 6.7, the association of  $[\text{Ru}(\text{bpy})_3]^{2+}$  with the surface is much stronger at equivalent  $[\text{Ru}(\text{bpy})_3]^{2+}$  concentrations, particularly when supporting electrolyte is absent. This can be attributed to the increase in the density of adsorption sites on the negatively charged polymer. Furthermore, the surface concentration of  $[\text{Ru}(\text{bpy})_3]^{2+}$

on PLL/PGA approaches monolayer coverage at much lower bulk concentration compared to similar experiments on silica, again notably with supporting electrolyte absent.

Comparing Figures 5A and 5B, it can be seen that the addition of supporting electrolyte has a significant impact in decreasing the  $[\text{Ru}(\text{bpy})_3]^{2+}$  surface concentration, so that monolayer coverage requires a much higher bulk concentration of  $[\text{Ru}(\text{bpy})_3]^{2+}$  (note the difference in the concentration ranges of the plots in Figures 5A and 5B). With supporting electrolyte present, the charge of some of the deprotonated acid groups of PGA will be partially screened by the large excess of  $\text{TBA}^+$  ions, and a higher concentration of  $[\text{Ru}(\text{bpy})_3]^{2+}$  is needed in bulk to promote surface adsorption.

The experimental data for adsorption of  $[\text{Ru}(\text{bpy})_3]^{2+}$  to PLL/PGA functionalized silica were fitted to a Langmuir isotherm:

$$A = A_{\max} \frac{K c_{\text{Ru}}}{1 + K c_{\text{Ru}}}, \quad (4)$$

where  $A_{\max}$  is the maximum optical absorbance for the adsorbed phase and  $K$  again represents the equilibrium adsorption constant. The best fitting parameters were  $A_{\max} = 0.0023$  and  $K = 2.89 \times 10^5 \text{ M}^{-1}$  with no supporting electrolyte in solution, and  $A_{\max} = 0.0021$  and  $K = 3.85 \times 10^3 \text{ M}^{-1}$  with 50 mM TBACl.

The pH-dependence of the surface concentration of  $[\text{Ru}(\text{bpy})_3]^{2+}$  on the PLL/PGA functionalized surface from a solution of 0.1 mM  $[\text{Ru}(\text{bpy})_3]^{2+}$  without electrolyte is shown in Figure 6. The shape of the curve resembles the titration behavior of a weak acid. The curve is fitted to:<sup>80</sup>

$$A = A_{\max} \frac{1}{1 + 10^{pK_a - \text{pH}}} + A_{\text{bulk}} \quad (5)$$

which gives  $A_{\max} = 4.2 \times 10^{-3}$  and the surface  $pK_a = 5.5$  which is 1.2 pH units higher than the  $pK_a$  of glutamic acid.<sup>81</sup> This increase in  $pK_a$  of acid groups upon surface confinement

has been seen previously, for example in the work of Bryant and Crooks,<sup>82</sup> and can be attributed to intramonolayer interactions and double layer effects.

**Dynamic adsorption/desorption measurements.** It is clear from the results above that the extent of the adsorption of  $[\text{Ru}(\text{bpy})_3]^{2+}$  on various interfaces is strongly pH-dependent. The use of dynamic electrochemistry to change the pH would open up several interesting possibilities in adsorption studies, notably the possibility of accessing adsorption/desorption kinetics or measuring pH-dependent isotherms more rapidly than in the static studies described above. By positioning a working macroelectrode close to the prism surface the pH can be changed locally by the anodic oxidation of water. We have shown previously for steady-state conditions at ultramicroelectrodes that this is a well-defined process.<sup>71</sup> Here, we characterize time-dependent proton generation at a large electrode.

In order to determine the pH at the prism surface from the anodic oxidation of water, CSLM was used to monitor the fluorescence of fluorescein as a pH indicator. Fluorescein is a fluorophore whose fluorescence intensity varies sigmoidally from 0 to 100 % within the pH region 4-7.<sup>71</sup> By performing a line scan in the gap between the electrode and a glass substrate (mimicking the prism surface) at the center of the electrode, the fluorescence intensity could be monitored during the production of protons resulting from the chronoamperometric potential step experiment. The intensity could then be used to determine the pH between the electrode and substrate using a calibration curve of fluorescence intensity versus pH similar to that shown previously (Figure 3 in Rudd *et al.*<sup>71</sup>). Typical data from this experiment are shown in Figure 7. Figure 7B shows the current response of the electrode due to the applied potential profile shown in Figure 7A. The forward potential step, from 0.2 V to 1.2 V for 2 s, results in an anodic current transient that is accompanied by a change in fluorescence signal at the electrode surface from light



to dark, which spreads into the solution as electrogenerated protons diffuse towards the substrate. The reverse potential step is accompanied by a small cathodic current transient with time, the fluorescence signal in the gap between the electrode and substrate gradually decreases, consistent with proton generation.

Typical examples of the change in pH at the glass substrate, with time, for different electrode-prism separations and potential step times are shown in Figure 8. The measured relative absorbance was converted to pH using a fluorescence intensity-pH plot similar to that reported in Rudd *et al.*<sup>71</sup> It can be seen that after a lag time which depends on the electrode to glass surface separation, the pH abruptly decreases over a period of 1-2 s and reaches a fairly steady value. The value attained following the potential perturbation clearly depends on the duration of the pulse and the thickness of the cell: a shorter pulse and thicker cell yield smaller changes in pH.

With a detailed knowledge of the pH from these measurements it was possible to carry out similar potential-induced proton generation in the EW-CRDS configuration. Figure 9A shows typical EW-CRDS absorbance-time plots for a potential step from 0.2 V to 1.2 V and back to 0.2 V vs. Ag/AgCl for different prism/electrode separation distances and pulse generation times. In each case there is a decrease in absorbance following the electrochemical generation of H<sup>+</sup>, the morphology of the curves is similar to the CSLM data, showing a strong dependence on pulse width and electrode/prism separation. The larger the separation, the longer the lag time, and the smaller the change in optical absorbance. Likewise, for a given electrode/prism separation, the shorter the pulse width, the smaller the overall pH change and thus the smaller the extent of [Ru(bpy)<sub>3</sub>]<sup>2+</sup> desorption. This is consistent with proton generation at the electrode causing desorption of [Ru(bpy)<sub>3</sub>]<sup>2+</sup> from the substrate surface.

The CSLM data yield interfacial pH as a function of time, whilst EW-CRDS yields  $\Gamma$  vs. time. From this we can construct  $\Gamma$ -pH plots, typical examples of which can be seen in Figure 10. We may further consider that acid-induced desorption is rather rapid on the timescale of these measurements, so that the amount of  $[\text{Ru}(\text{bpy})_3]^{2+}$  on the surface is governed by the local pH. The  $\Gamma$ -pH plots can then be analyzed using equation 5. The data in Figure 10A and 10B gave best fits to  $pK_a$  of 5.5 and 5.9 respectively. The mean  $pK_a$  from all data sets was  $5.6 \pm 0.3$  which is in good agreement with the equilibrium pH dependence measurements shown in Figure 6.

## Conclusions

EW-CRDS has proven to be a valuable technique for probing the pH-dependent adsorption of  $[\text{Ru}(\text{bpy})_3]^{2+}$  on silica, PLL and a PLL/PGA bilayer. In the case of silica and PLL/PGA, Langmuir-type adsorption isotherms were observed with the adsorption being strongly pH-dependent and influenced by the addition of supporting electrolyte. In contrast, the positively charged PLL surface effectively prevented any adsorption of  $[\text{Ru}(\text{bpy})_3]^{2+}$ .

By combining EW-CRDS with chronoamperometry at an electrode positioned just above the prism surface, the pH could be changed rapidly and quantitatively. By varying the potential step times for proton generation and the electrode/prism separation, it was possible to obtain information on the pH-dependent adsorption of  $[\text{Ru}(\text{bpy})_3]^{2+}$  on the carboxylic-acid terminated surface. Combined with CSLM to obtain quantitative information on the pH at the prism surface, the adsorption/desorption process was shown to be governed by the protonation/deprotonation of the PGA film and the surface  $pK_a$  of the film was found to be 5.6 consistent with the static pH-titration measurements.

We have demonstrated the combination of EW-CRDS with electrochemical techniques to probe dynamic adsorption/desorption processes on an electrically insulating macroscopic substrate. The list of potential applications of this novel combination of electrochemistry and optical spectroscopy is large and varied, but we envisage it will be especially useful for investigating interfacial kinetics of processes such as dissolution/growth and surface processes in the life sciences such as protein interactions with biological membranes.

## References

- (1) Adamson, A. W.; Gast, A. P., 6th ed.; John Wiley & Sons Inc., 1997.
- (2) Ballschmiter, K. *Angewandte Chemie-International Edition in English* **1992**, *31*, 487-515.
- (3) Bard, A. J.; Faulkner, L. R., 2nd ed.; John Wiley & Sons Inc., 2004.
- (4) Dabrowski, A. *Advances in Colloid and Interface Science* **2001**, *93*, 135-224.
- (5) Huang, C. P. In *Adsorption of Inorganics at the Solid-Liquid Interface*; Anderson, M. A., Rubin, A. J., Eds.; Ann Arbor Science: Ann Arbor, MI, 1981, pp 183-217.
- (6) Nawrocki, J. *Chromatographia* **1991**, *31*, 177-192.
- (7) Nawrocki, J. *Journal of Chromatography A* **1997**, *779*, 29-71.
- (8) Siejko, F. L. *Adsorption Technology*; Marcel Dekker: New York, 1985.
- (9) Haddad, P. R.; Jackson, P. E. *Ion Chromatography: Principles and Applications*; Elsevier, 1990.
- (10) Al-Abadleh, H. A.; Mifflin, A. L.; Musorrafiti, M. J.; Geiger, F. M. *Journal of Physical Chemistry B* **2005**, *109*, 16852-16859.
- (11) Camillone, N. *Langmuir* **2004**, *20*, 1199-1206.
- (12) Ji, X. B.; Chevallier, F. G.; Clegg, A. D.; Buzzeo, M. C.; Compton, R. G. *Journal of Electroanalytical Chemistry* **2005**, *581*, 249-257.
- (13) Norman, L. L.; Badia, A. *Langmuir* **2007**, *23*, 10198-10208.
- (14) Schon, P.; Gorlich, M.; Coenen, M. J. J.; Heus, H. A.; Speller, S. *Langmuir* **2007**, *23*, 9921-9923.
- (15) Damian, A.; Omanovic, S. *Langmuir* **2007**, *23*, 3162-3171.
- (16) Enders, D.; Nagao, T.; Nakayama, T.; Aono, M. *Langmuir* **2007**, *23*, 6119-6125.
- (17) Frateur, I.; Lecoer, J.; Zanna, S.; Olsson, C. O. A.; Landolt, D.; Marcus, P. *Electrochimica Acta* **2007**, *52*, 7660-7669.
- (18) Climent, V.; Coles, B. A.; Compton, R. G. *Journal of Physical Chemistry B* **2002**, *106*, 5988-5996.
- (19) Ikeda, T.; Nakahara, J.; Sasaki, M.; Yasunaga, T. *Journal of Colloid and Interface Science* **1984**, *97*, 278-283.
- (20) Bujalski, R.; Cantwell, F. F. *Analytical Chemistry* **2006**, *78*, 1593-1605.
- (21) Strelow, F.; Henglein, A. *Journal of Physical Chemistry* **1995**, *99*, 11834-11838.
- (22) Taniguchi, M.; Kaneyoshi, M.; Nakamura, Y.; Yamagishi, A.; Iwamoto, T. *Journal of Physical Chemistry* **1990**, *94*, 5896-5900.

- (23) Liu, C.; Huang, P. M. *Geoderma* **2001**, *102*, 1-25.
- (24) Wu, C. H.; Lin, C. F.; Lo, S. L.; Yasunaga, T. *Journal of Colloid and Interface Science* **1998**, *208*, 430-438.
- (25) Hachiya, K.; Sasaki, M.; Ikeda, T.; Mikami, N.; Yasunaga, T. *J. Phys. Chem.* **1984**, *88*, 27-31.
- (26) Compton, R. G.; Pritchard, K. L. *Journal of the Chemical Society-Faraday Transactions* **1990**, *86*, 129-136.
- (27) Burt, D. P.; Cervera, J.; Mandler, D.; Macpherson, J. V.; Manzanares, J. A.; Unwin, P. R. *Physical Chemistry Chemical Physics* **2005**, *7*, 2955-2964.
- (28) Mansikkamaki, K.; Haapanen, U.; Johans, C.; Kontturi, K.; Valden, M. *Journal of the Electrochemical Society* **2006**, *153*, B311-B318.
- (29) Unwin, P. R.; Bard, A. J. *Journal of Physical Chemistry* **1992**, *96*, 5035-5045.
- (30) Unwin, P. R.; Bard, A. J. *Analytical Chemistry* **1992**, *64*, 113-119.
- (31) Ball, S. M.; Jones, R. L. *Chemical Reviews* **2003**, *103*, 5239-5262.
- (32) Berden, G.; Peeters, R.; Meijer, G. *International Reviews in Physical Chemistry* **2000**, *19*, 565-607.
- (33) Scherer, J. J.; Paul, J. B.; Okeefe, A.; Saykally, R. J. *Chemical Reviews* **1997**, *97*, 25-51.
- (34) Vallance, C. *New Journal of Chemistry* **2005**, *29*, 867-874.
- (35) Hallock, A. J.; Berman, E. S. F.; Zare, R. N. *Analytical Chemistry* **2002**, *74*, 1741-1743.
- (36) Hallock, A. J.; Berman, E. S. F.; Zare, R. N. *Analytical Chemistry* **2007**, *79*, 2596-2596.
- (37) Kleine, D.; Lauterbach, J.; Kleinermanns, K.; Hering, P. *Applied Physics B-Lasers and Optics* **2001**, *72*, 249-252.
- (38) Alexander, A. J. *Chemical Physics Letters* **2004**, *393*, 138-142.
- (39) Snyder, K. L.; Zare, R. N. *Analytical Chemistry* **2003**, *75*, 3086-3091.
- (40) Xu, S. C.; Sha, G. H.; Xie, J. C. *Review of Scientific Instruments* **2002**, *73*, 255-258.
- (41) Pipino, A. C. R.; Hudgens, J. W.; Huie, R. E. *Review of Scientific Instruments* **1997**, *68*, 2978-2989.
- (42) Pipino, A. C. R.; Hoefnagels, J. P. M.; Watanabe, N. *Journal of Chemical Physics* **2004**, *120*, 2879-2888.
- (43) Hannon, T. E.; Chah, S. W.; Zare, R. N. *Journal of Physical Chemistry B* **2005**, *109*, 7435-7442.
- (44) Fisk, J. D.; Batten, R.; Jones, G.; O'Reilly, J. P.; Shaw, A. M. *Journal of Physical Chemistry B* **2005**, *109*, 14475-14480.
- (45) O'Reilly, J. P.; Butts, C. P.; I'Anson, I. A.; Shaw, A. M. *Journal of the American Chemical Society* **2005**, *127*, 1632-1633.
- (46) Shaw, A. M.; Hannon, T. E.; Li, F. P.; Zare, R. N. *Journal of Physical Chemistry B* **2003**, *107*, 7070-7075.
- (47) Everest, M. A.; Black, V. M.; Haehlen, A. S.; Haveman, G. A.; Kliewer, C. J.; Neill, H. A. *Journal of Physical Chemistry B* **2006**, *110*, 19461-19468.
- (48) Fan, H. F.; Hung, C. Y.; Lin, K. C. *Analytical Chemistry* **2006**, *78*, 3583-3590.
- (49) Mazurenka, M.; Wilkins, L.; Macpherson, J. V.; Unwin, P. R.; Mackenzie, S. R. *Analytical Chemistry* **2006**, *78*, 6833-6839.
- (50) Fan, H. F.; Li, F.; Zare, R. N.; Lin, K. C. *Anal. Chem.* **2007**, *79*, 3654-3661.
- (51) Pipino, A. C. R. *Physical Review Letters* **1999**, *83*, 3093-3096.
- (52) Pipino, A. C. R. *Applied Optics* **2000**, *39*, 1449-1453.

- (53) Pipino, A. C. R.; Hudgens, J. W.; Huie, R. E. *Chemical Physics Letters* **1997**, 280, 104-112.
- (54) Aarts, I. M. P.; Pipino, A. C. R.; Hoefnagels, J. P. M.; Kessels, W. M. M.; van de Sanden, M. C. M. *Physical Review Letters* **2005**, 95.
- (55) Tarsa, P. B.; Rabinowitz, P.; Lehmann, K. K. *Chemical Physics Letters* **2004**, 383, 297-303.
- (56) Pipino, A. C. R.; Michalski, M. *Journal of Physical Chemistry C* **2007**, 111, 9442-9447.
- (57) Li, F. P.; Zare, R. N. *Journal of Physical Chemistry B* **2005**, 109, 3330-3333.
- (58) Mazurenka, M.; Hamilton, S. M.; Unwin, P. R.; Mackenzie, S. R. *Journal of Physical Chemistry C* **2008**, 112, 6462-6468.
- (59) Schnippering, M.; Powell, H. V.; Zhang, M.; Macpherson, J. V.; Unwin, P. R.; Mazurenka, M.; Mackenzie, S. R. *Journal of Physical Chemistry C* **2008**, *In press*.
- (60) Dennany, L.; O'Reilly, E. J.; Keyes, T. E.; Forster, R. J. *Electrochemistry Communications* **2006**, 8, 1588-1594.
- (61) Gerardi, R. D.; Barnett, N. W.; Lewis, S. W. *Analytica Chimica Acta* **1999**, 378, 1-41.
- (62) Zhuang, Y. F.; Ju, H. X. *Electroanalysis* **2004**, 16, 1401-1405.
- (63) Choi, H. N.; Yoon, S. H.; Lyu, Y. K.; Lee, W. Y. *Electroanalysis* **2007**, 19, 459-465.
- (64) Bertonecello, P.; Dennany, L.; Forster, R. J.; Unwin, P. R. *Analytical Chemistry* **2007**, 79, 7549-7553.
- (65) Liang, M. M.; Liu, S. L.; Wei, M. Y.; Guo, L. H. *Analytical Chemistry* **2006**, 78, 621-623.
- (66) Kuwahara, Y.; Akiyama, T.; Yamada, S. *Thin Solid Films* **2001**, 393, 273-277.
- (67) Chaturvedi, H.; Poler, J. C. *Journal of Physical Chemistry B* **2006**, 110, 22387-22393.
- (68) Bottini, M.; Magrini, A.; Di Venere, A.; Bellucci, S.; Dawson, M. I.; Rosato, N.; Bergamaschi, A.; Mustelin, T. *Journal of Nanoscience and Nanotechnology* **2006**, 6, 1381-1386.
- (69) Zhuang, Y. F.; Ju, H. X. *Analytical Letters* **2005**, 38, 2077-2088.
- (70) Kuang, D.; Klein, C.; Snaith, H. J.; Humphry-Baker, R.; Zakeeruddin, S. M.; Gratzel, M. *Inorganica Chimica Acta* **2008**, 361, 699-706.
- (71) Rudd, N. C.; Cannan, S.; Bitziou, E.; Ciani, L.; Whitworth, A. L.; Unwin, P. R. *Analytical Chemistry* **2005**, 77, 6205-6217.
- (72) Mazurenka, M.; Wada, R.; Shillings, A. J. L.; Butler, T. J. A.; Beames, J. M.; Orr-Ewing, A. J. *Applied Physics B-Lasers and Optics* **2005**, 81, 135-141.
- (73) Eisenberg, M.; Gresalfi, T.; Riccio, T.; McLaughlin, S. *Biochemistry* **1979**, 18, 5213-5223.
- (74) Macpherson, J. V.; Beeston, M. A.; Unwin, P. R. *Journal of the Chemical Society-Faraday Transactions* **1995**, 91, 899-904.
- (75) Bitziou, E.; Rudd, N. C.; Edwards, M. A.; Unwin, P. R. *Analytical Chemistry* **2006**, 78, 1435-1443.
- (76) Cannan, S.; Macklam, I. D.; Unwin, P. R. *Electrochemistry Communications* **2002**, 4, 886-892.
- (77) Harrick, N. J.; Carlson, A. I. *Applied Optics* **1971**, 10, 19-&.
- (78) Dong, Y.; Pappu, S. V.; Xu, Z. *Analytical Chemistry* **1998**, 70, 4730-4735.
- (79) Cox, G. B. *Journal of Chromatography A* **1993**, 656, 353-367.

- (80) Zhao, X.; Ong, S.; Wang, H.; Eisenthal, K. B. *Chemical Physics Letters* **1993**, 214, 203-207.
- (81) In *CRC Handbook of Chemistry and Physics*, 88th ed.; Lide, D. R., Ed.; CRC Press.
- (82) Bryant, M. A.; Crooks, R. M. *Langmuir* **1993**, 9, 385-387.

## Figure Captions

Figure 1: Experimental setup for electrochemical EW-CRDS studies. Light from a rapid pulsed broadband diode laser (2.4kHz, 1nm FWHM) is injected into a ring cavity comprising two high reflective mirrors and the total internal reflection surface of a right angled prism. The ring-down of the light in the cavity is recorded by the photomultiplier tube (PMT).

Figure 2: Concentration dependence of  $[\text{Ru}(\text{bpy})_3]^{2+}$  optical absorbance above a PLL-modified silica surface in i) pure water (blue squares) and ii) 50mM TBACl (red triangles). The positively charged surface prevents adsorption of  $[\text{Ru}(\text{bpy})_3]^{2+}$  and the absorbance measured corresponds to bulk solution absorbance with an effective thickness of 1.08  $\mu\text{m}$ .

Figure 3: A) Typical optical absorbance transients for  $[\text{Ru}(\text{bpy})_3]^{2+}$  with a silica substrate as the base of the cell. The concentrations and pH were 0.5 mM, pH 2.7 (bottom, green) and 1 mM, pH 2.7 (middle, blue) and 1 mM, pH 6.7 (top, red) B) Concentration

dependence of  $[\text{Ru}(\text{bpy})_3]^{2+}$  optical absorbance on bare silica as the base of the cell at i) pH 2.7 (red squares) and ii) 6.7 (blue triangles).

Figure 4: pH-dependence (recorded in the direction of increasing pH) of  $[\text{Ru}(\text{bpy})_3]^{2+}$  adsorption on bare silica in i) pure water (blue triangles) and ii) 0.1 M NaCl (red squares). Bulk  $[\text{Ru}(\text{bpy})_3]^{2+}$  concentration was 1 mM.

Figure 5: Surface concentration of  $[\text{Ru}(\text{bpy})_3]^{2+}$  achieved on PLL/PGA-modified silica as a function of bulk concentration in A) pure water (blue triangles) and B) 50 mM TBACl (red squares), both at pH 8.

Figure 6: pH-dependence of  $[\text{Ru}(\text{bpy})_3]^{2+}$  surface concentration on PLL/PGA-modified silica from pure water. The bulk  $[\text{Ru}(\text{bpy})_3]^{2+}$  concentration was 0.1 mM.

Figure 7: Electrochemically-induced  $[\text{Ru}(\text{bpy})_3]^{2+}$  desorption from a substrate. (A) The potential applied to the working electrode as a function of time and (B) the corresponding current response. (C) The corresponding series of CLSM linescans between the electrode (blue area at the top) and the glass substrate (blue area at the bottom) as a function of time are shown. Relatively high fluorescence corresponds to pH > 7.

Figure 8: Transients showing the pH at the prism surface as determined from CLSM after applying a potential of +1.2 V vs. Ag/AgCl: (A) for 2s at different prism/electrode distances (from bottom to top) of i) 300  $\mu\text{m}$  (red), ii) 400  $\mu\text{m}$  (blue); (B) for an electrode-prism separation of 200  $\mu\text{m}$  for (from top to bottom) (i) 100 ms (red), ii) 250 ms (blue), iii) 500 ms (green), iv) 1 s (orange) .

Figure 9: Optical absorbance transients of surface-adsorbed  $[\text{Ru}(\text{bpy})_3]^{2+}$  from a bulk solution of 50  $\mu\text{M}$   $[\text{Ru}(\text{bpy})_3]^{2+}$  on PGA after applying a potential of +1.2 V vs. Ag/AgCl:

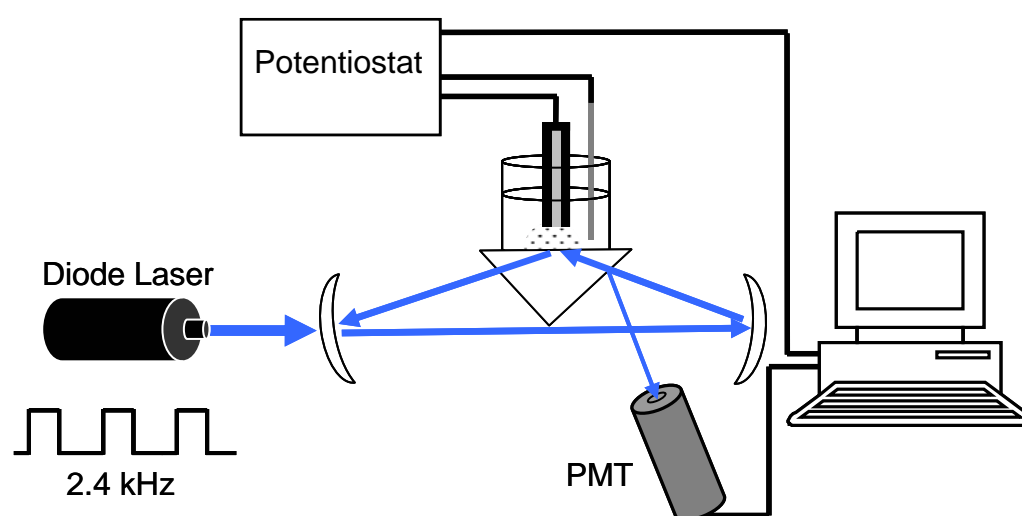
(A) for 2 s at different prism/electrode distances (from bottom to top) of i) 300  $\mu\text{m}$  (red), ii) 400  $\mu\text{m}$  (blue), iii) 500  $\mu\text{m}$  (green) and (B) for an electrode-prism distance of 200  $\mu\text{m}$  and pulse times of i) 100 ms (red), ii) 250 ms (blue), iii) 500 ms (green), iv) 1 s (orange) .

Figure 10: Typical plots of optical absorbance for surface-confined  $[\text{Ru}(\text{bpy})_3]^{2+}$  on PGA versus pH determined from the CLSM measurements. (A) Electrode-prism separation of 400  $\mu\text{m}$  and 2 second potential step time. The red line is the fit to equation 5 with  $pK_a = 5.5$ . (B) is for an electrode-prism separation of 200  $\mu\text{m}$  and 100 ms potential step time. The red line is the fit to equation 5 with  $pK_a = 5.9$ .



## Figures

Figure 1



**Figure 2**

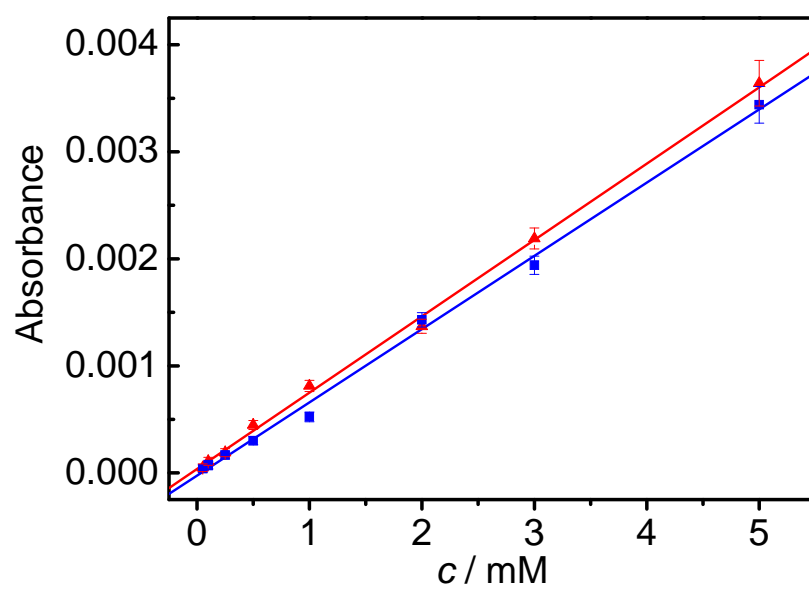


**Figure 3**

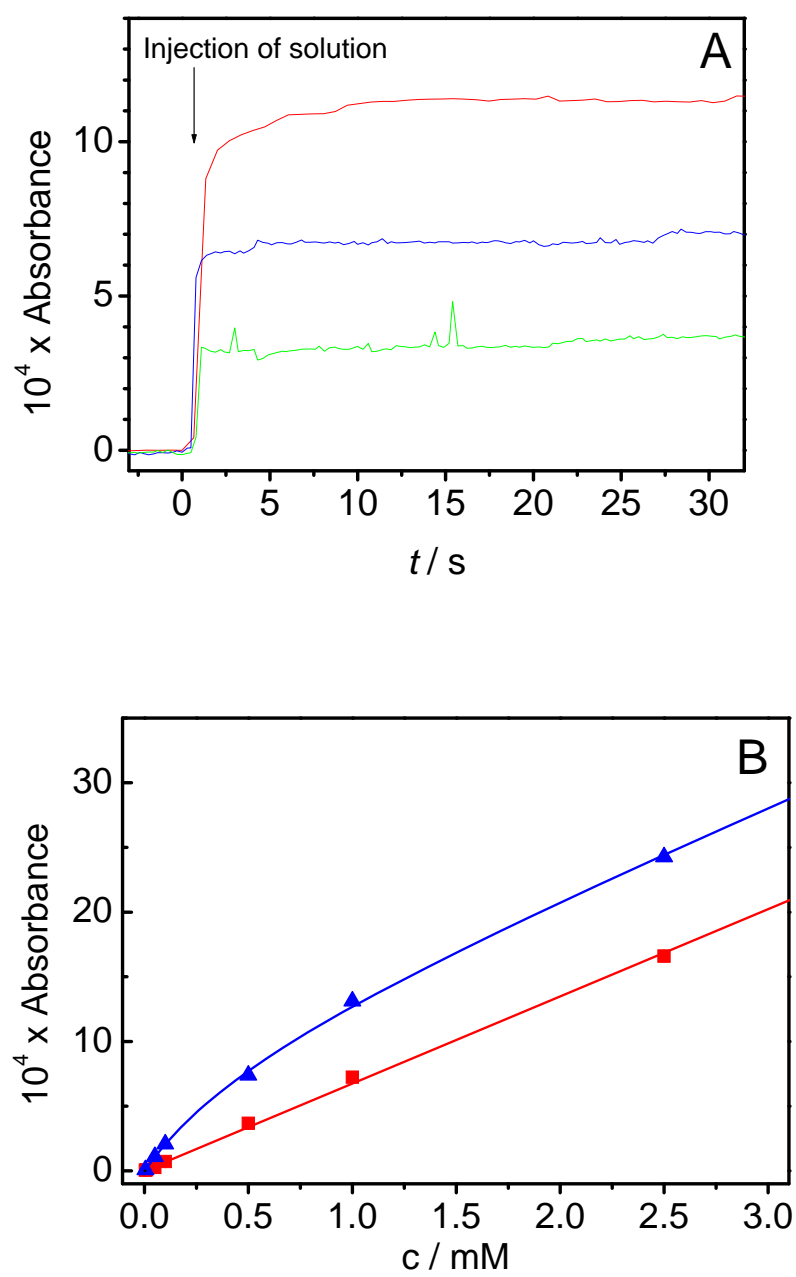


**Figure 4**

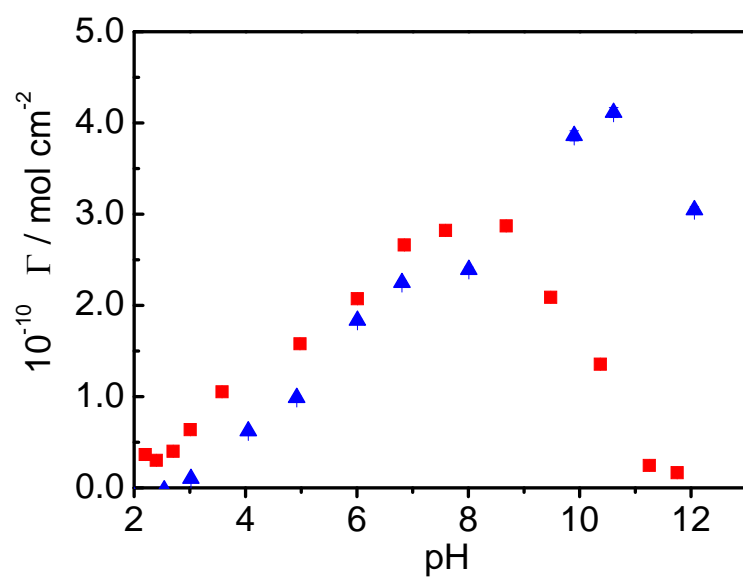


**Figure 5**

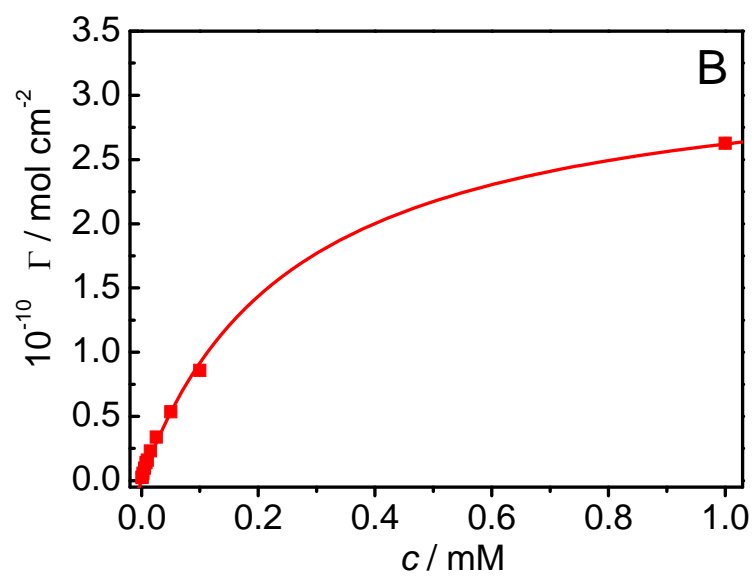
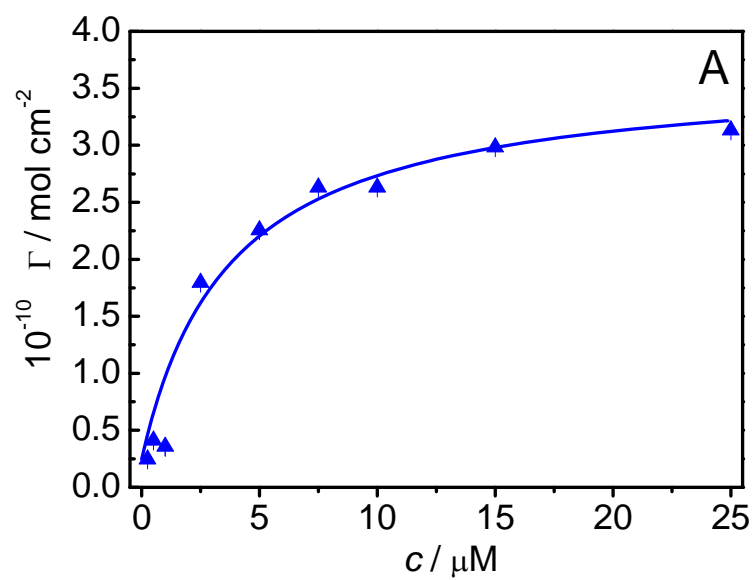


**Figure 6**

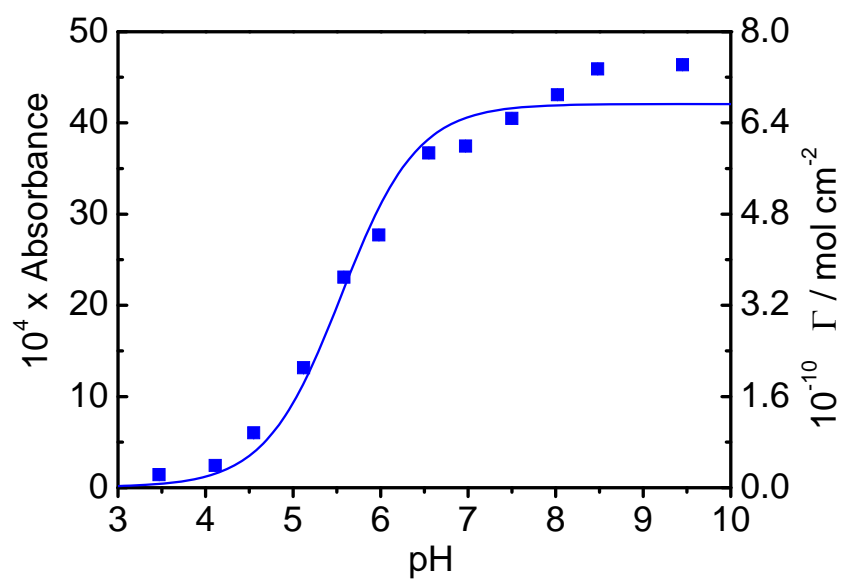


**Figure 7**

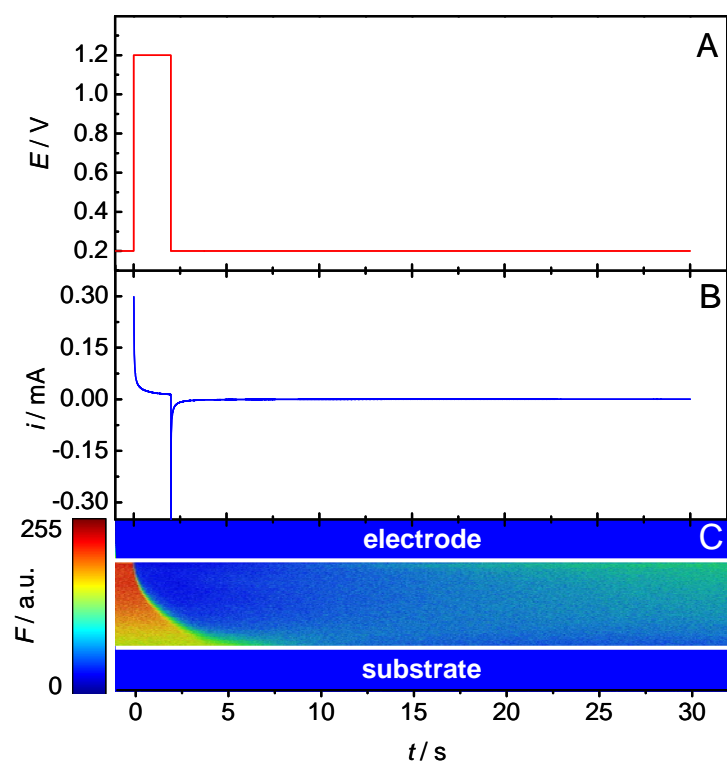


**Figure 8**

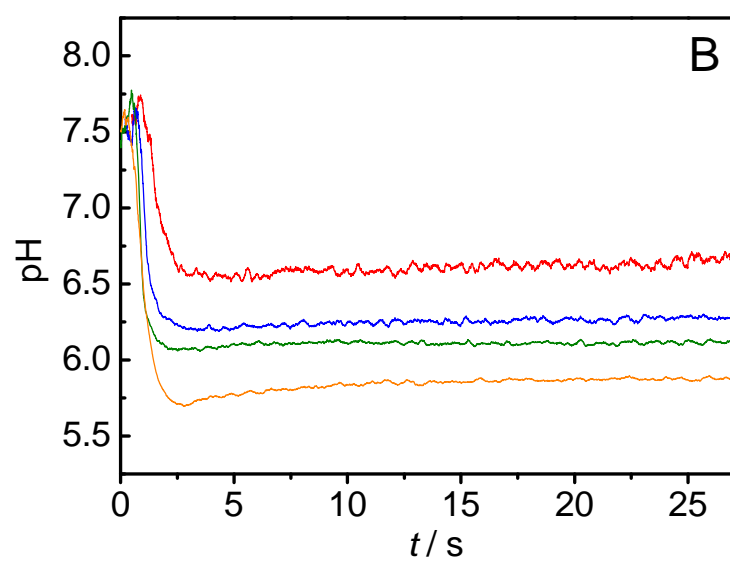
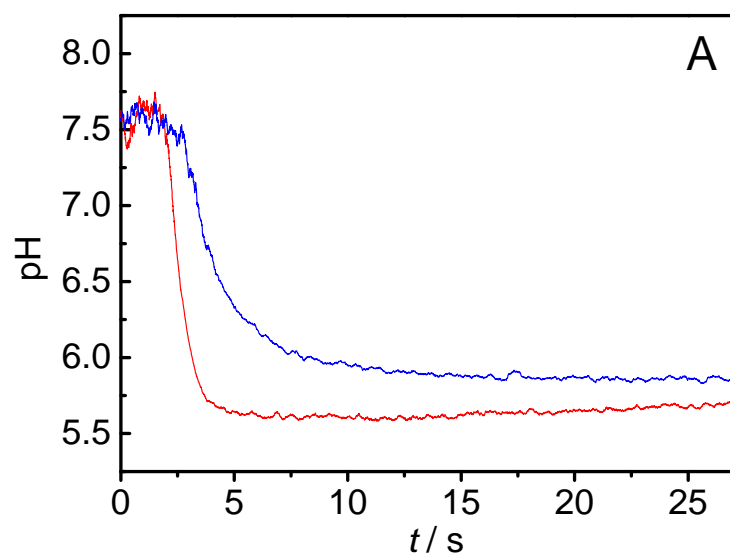




**Figure 9**

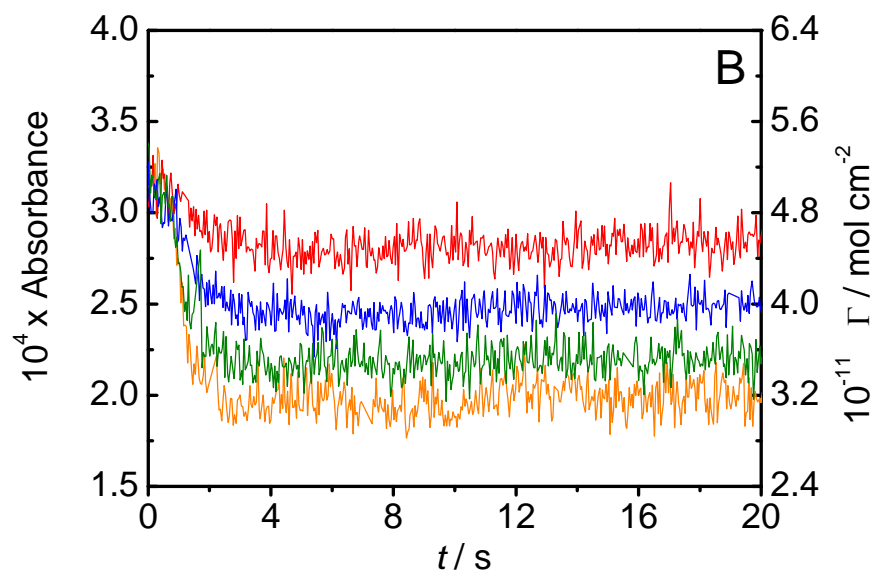
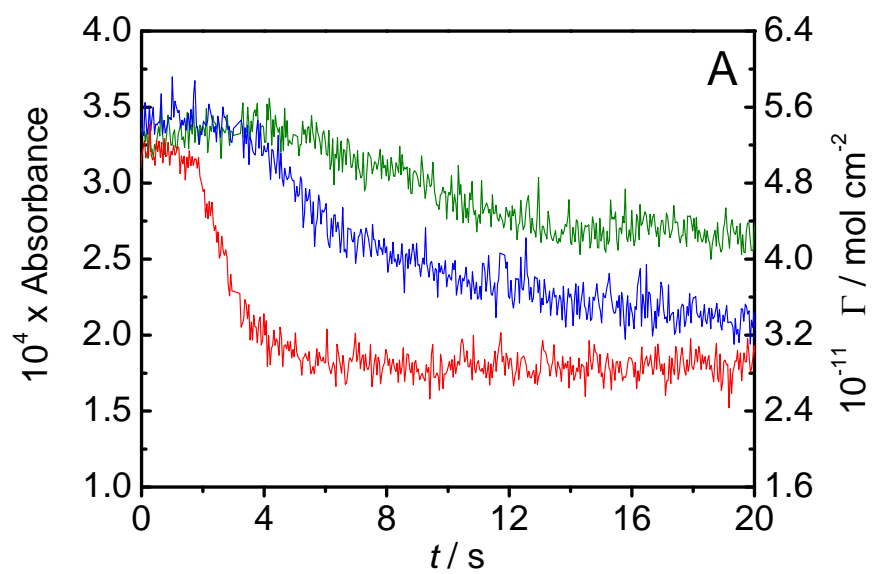


**Figure 10**

